



# Nutrient trapping in the equatorial Pacific: The ocean circulation solution

Olivier Aumont, James C. Orr, Patrick Monfray, Gurvan Madec

## ► To cite this version:

Olivier Aumont, James C. Orr, Patrick Monfray, Gurvan Madec. Nutrient trapping in the equatorial Pacific: The ocean circulation solution. [0] Notes scientifiques du Pôle de modélisation du climat. 5, IPSL. 1998. hal-03319585

**HAL Id: hal-03319585**

**<https://hal.science/hal-03319585>**

Submitted on 12 Aug 2021

**HAL** is a multi-disciplinary open access archive for the deposit and dissemination of scientific research documents, whether they are published or not. The documents may come from teaching and research institutions in France or abroad, or from public or private research centers.

L'archive ouverte pluridisciplinaire **HAL**, est destinée au dépôt et à la diffusion de documents scientifiques de niveau recherche, publiés ou non, émanant des établissements d'enseignement et de recherche français ou étrangers, des laboratoires publics ou privés.

# Institut Pierre Simon Laplace

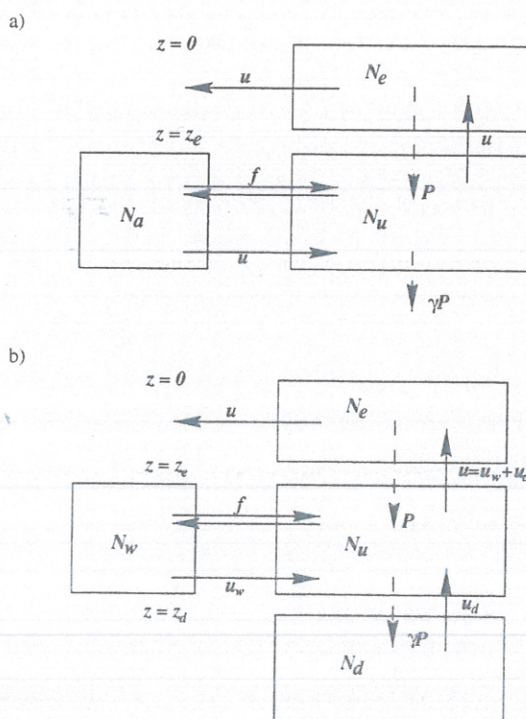
des Sciences de l'Environnement Global

## Notes du Pôle de Modélisation

### Nutrient trapping in the equatorial Pacific: The ocean circulation solution

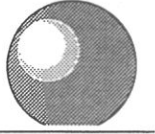
O. Aumont(1), J. C. Orr(1), P. Monfray(1), and G. Madec(2)

(1) Laboratoire des Sciences du Climat et de l'Environnement,  
(2) Laboratoire d'Océanographie Dynamique et de Climatologie







|   |  |
|---|--|
| <br>I P S L  | <p align="center"> <b>CNRS - Université Pierre et Marie Curie - Université<br/>Versailles-Saint-Quentin</b><br/> <b>CEA - CNES - ORSTOM - Ecole Normale Supérieure - Ecole<br/>Polytechnique</b><br/> <br/> <b>Institut Pierre Simon Laplace</b><br/> <b>des Sciences de l'Environnement Global</b><br/> <br/> <b>CETP - LMD - LODYC - LPCM - LSCE - SA</b> </p> |
| <b>Université Pierre-et-Marie-Curie</b><br>B 102 - T15-E5 - 4, Place Jussieu<br>75252 Paris Cedex 05 (France)<br>Tél : (33) 01 44 27 39 83<br>Fax : (33) 01 44 27 37 76 | <p align="right"> <b>Université Versailles-Saint-Quentin</b><br/>         Collège Vauban, 47 Boulevard Vauban<br/>         78047 Guyancourt Cedex (France)<br/>         Tél : (33) 01 39 25 58 17<br/>         Fax : (33) 01 39 25 58 22       </p>  |

## Nutrient trapping in the equatorial Pacific: The ocean circulation solution

O. Aumont(1), J. C. Orr(1), P. Monfray(1), and G. Madec(2)

(1) Laboratoire des Sciences du Climat et de l'Environnement,

(2) Laboratoire d'Océanographie Dynamique et de Climatologie

Le "nutrient trapping" est un défaut classique des modèles globaux du cycle du carbone utilisant un schéma d'export seulement basé sur les particules. Défini comme une accumulation excessive des nutriments en sub-surface par rapport aux observations, celui-ci survient principalement dans l'est de l'océan Pacifique équatorial. Les études précédentes se sont efforcées de résoudre ce problème en accroissant la complexité des modèles biogéochimiques utilisés. Ici, nous montrons que, plutôt que la biogéochimie, des défauts dans la circulation simulée par les modèles de basse résolution en sont à l'origine. Cette nouvelle analyse provient de notre utilisation d'un modèle océanique de circulation générale de plus haute résolution que ceux qui ont été classiquement utilisés jusque là. Par ailleurs, nous avons utilisé le même modèle biogéochimique simple HAMOCC3 (Hamburg ocean carbon cycle model-version 3) que dans certaines des études précédentes. La distribution simulée des phosphate dans l'océan Pacifique équatorial est en assez bon accord avec les observations et ce, aussi bien en surface qu'en sub-surface. ../..

|                                       |
|---------------------------------------|
| <b>Avril 1998</b><br><b>Note n° 5</b> |
|---------------------------------------|





Dans l'est de l'océan Pacifique équatorial, les concentrations en sub-surface des phosphate prédites par le modèle ne dépassent pas de plus de 15 l'inverse des modèles de plus basse résolution. Cette amélioration est due à une meilleure résolution méridienne (0,5°) près de l'équateur, qui permet au modèle de représenter de façon adéquate le vigoureux sous-courant équatorial, ce dernier apportant des eaux faiblement chargées en nutriments depuis l'est du bassin. En outre, le modèle ne produit pas une remontée d'eaux abyssales riches en nutriments à travers la thermocline, par la suite injectées en surface de l'océan Pacifique équatorial. Nos résultats suggèrent que le DOC joue un faible rôle dans le budget de carbone de l'océan Pacifique équatorial.





# Nutrient trapping in the equatorial Pacific: The ocean circulation solution.

O. Aumont<sup>1</sup>, J. C. Orr<sup>1</sup>, P. Monfray<sup>2</sup>, and G. Madec<sup>3</sup>

<sup>1</sup>Laboratoire de Modélisation du Climat et de l'Environnement, DSM, CE Saclay, CEA, L'Orme des Merisiers, Bât. 709, F-91191 Gif sur Yvette, Cedex, France

<sup>2</sup>Centre des Faibles Radioactivités, Laboratoire mixte CNRS-CEA, L'Orme des Merisiers, Bât. 709/LMCE, CE Saclay, F-91191 Gif sur Yvette, Cedex, France

<sup>3</sup>Laboratoire d'Océanographie Dynamique et de Climatologie, (CNRS/ORSTOM/UPMC) Université Paris VI, 4 place Jussieu, Paris, France

Short title: NUTRIENT TRAPPING: A DYNAMIC SOLUTION

Abstract. Nutrient trapping is a chronic problem found in global carbon-cycle models with particle-only remineralization schemes. It is defined as the excess of sub-surface nutrient relative to observations and occurs principally in the eastern equatorial Pacific. Previous studies have attempted to resolve simulated nutrient trapping by increasing the complexity of their modeled biogeochemistry. Here we show that deficiencies in modeled circulation fields from global coarse-resolution ocean models are mostly responsible. Our new interpretation stems from our use of an ocean general circulation model (OGCM) with higher resolution. We used the same biogeochemical model HAMOCC3 (Hamburg ocean carbon cycle model-version 3) as in some of the previous studies. Our model-predicted distribution of  $\text{PO}_4^{3-}$  in the equatorial Pacific agrees reasonably well with the observations both at the surface and in the sub-surface. Subsurface  $\text{PO}_4^{3-}$  concentrations in our model's eastern equatorial Pacific exceed observations by at most 15%, unlike coarser-resolution models. Improvement is due to enhanced meridional resolution ( $0.5^\circ$ ) near the equator, which allows the model to properly represent the vigorous equatorial undercurrent which brings in low nutrient water from the western basin. Furthermore, the model upwells no nutrient-rich abyssal water into the surface equatorial Pacific. Our results suggest that DOC plays a minor role in the carbon budget of the equatorial Pacific.

## 1. Introduction

The equatorial Pacific provides the largest source of  $\text{CO}_2$  from the ocean to the atmosphere. The wind-driven equatorial divergence drives  $\text{CO}_2$ -rich subsurface water to the surface, thereby inducing an outgassing of  $0.4\text{--}0.9 \text{ PgC yr}^{-1}$  [Gammon et al., 1985; Wong et al., 1993], mostly in the eastern and central basin. The corresponding large subsurface supply of nutrient maintains intense biological activity, perhaps representing up to to 58% of the global new production [Chavez and Barber, 1987]. Presumably the equatorial Pacific's new production could be even higher if the high levels of surface nutrients, abnormal for most of the ocean, could be used more efficiently. Production appears limited in the equatorial Pacific due to an insufficient supply of iron [Coale et al., 1996]. The equatorial Pacific is known for large interannual variability in ocean circulation and air-sea fluxes of  $\text{CO}_2$ . When upwelling weakens during El-Niño Southern Oscillation (ENSO) warm events, this source of  $\text{CO}_2$  may almost completely vanish [Wong et al., 1993].

Global coarse-resolution ocean models coupled to simple biogeochemical models have been used to improve understanding of the ocean's carbon cycle [Najjar, 1990; Bacastow and Maier-Reimer, 1991; Najjar et al., 1992; Maier-Reimer, 1993; Anderson and Sarmiento, 1995; Yamanaka and Tajika, 1996; Six and Maier-Reimer, 1996]. The first generation of such models includes a very simple particle-only remineralization scheme. Despite the ability of coarse-resolution circulation models in reproducing the large-scale features of observed tracers such as C-14, they all fail with particle-only remineralization scheme to simulate realistic nutrients near the equator. That is, they simulate high nutrient concentrations below areas of intense biological production; model-predicted nutrients exceed observations by at least 50% ( $1.5 \mu\text{mol L}^{-1}$ ), particularly in the eastern equatorial Pacific [Bacastow and Maier-Reimer, 1990; Najjar et al., 1992; Maier-Reimer, 1993]. Such a flaw, termed "nutrient trapping" by Najjar [1990], results from a positive feedback between intense production induced by the upwelling of nutrient-rich abyssal waters and remineralization of organic matter within the divergence.

To remedy this model artefact, efforts have focused entirely on apparent oversimplifications in modeled biogeochemistry. The first biogeochemical remedy for nutrient



trapping was motivated by new measurements of surprisingly large concentrations of DOC [Suzuki et al., 1985; Sugimura and Suzuki, 1988]. Ocean modelers who added a large, long-lived DOC pool to their particle-only models did indeed find substantial reduction in nutrient trapping [Najjar, 1990; Bacastow and Maier-Reimer, 1990; Najjar et al., 1992; Anderson and Sarmiento, 1995]. Analytical problems were eventually shown to be the cause of the high measured DOC [Suzuki, 1993]. Modelers had to find another solution.

Six and Maier-Reimer [1996] have proposed a second solution to nutrient trapping, but again have suggested that an oversimplified ocean biogeochemistry is responsible. To improve matters, their new biogeochemical model includes interactions between phytoplankton and zooplankton, as well as a reservoir of semi-labile DOC having a much shorter lifetime than that used previously. As a result, in the eastern equatorial Pacific ocean, the presence of a large standing stock of zooplankton reduces primary production and resulting export production. Additionally, a significant part of the organic matter is exported laterally as DOC away from the divergence. Combination of both factors (zooplankton grazing and horizontal DOC transport) reduces accumulation of nutrient below the divergence.

Another possibility, that faulty model circulation fields may cause nutrient trapping has not been explored previously. One reason is that separating out biogeochemical vs. dynamically driven problems is not easy to do with one model where both modules act together. To address this problem, we made new simulations in order to compare the effects of two very different circulation fields with one common biogeochemistry. For such, we have implanted the biogeochemical model HAMOCC3 developed by Maier-Reimer [1993] in OPA, an OGCM developed at the Laboratoire d'Océanographie Dynamique et de Climatologie (LODyC) in Paris. We then compared our results to those obtained with runs of HAMOCC3 in the LSG model from Maier-Reimer [1993].

We found that the OPA-HAMOCC3 model produces little nutrient trapping (model exceeds observed  $\text{PO}_4^{3-}$  by 15% at most); the LSG-HAMOCC3 combination [Maier-Reimer, 1993] produces larger excesses (up to 100%). In the equatorial Pacific, OPA's high resolution provides circulation fields that are more realistic. Critical features exhibited by OPA, but not by other coarse-resolution global OGCM's, include a vigorous

equatorial undercurrent and little upwelling of deep water to the surface. Further sensitivity tests demonstrate how nutrient trapping is sensitive to values of the horizontal eddy viscosity coefficients and thus to the resolution of the model.

## 2. Model Description

In this study, the ocean's preindustrial state, which is presumably at equilibrium, is simulated by implanting the Hamburg Ocean Carbon Cycle model-version 3 (HAMOCC3) [Maier-Reimer, 1993] into a tracer-transport model driven by 3-D advective and diffusive fields predicted by the OGCM known as OPA (océan parallélisé) [Delecluse et al., 1993]. Here we outline the important aspects of both models.

### 2.1. Ocean general circulation model

The OGCM used here was first developed a decade ago [Andrich, 1988]. Known as OPA, it has been modified for use as a regional [Blanke and Delecluse, 1993; Maes et al., 1997] and global-scale model [Marti, 1992; Delecluse et al., 1993; Madec and Imbard, 1996; Guilyardi and Madec, 1997]. OPA solves the primitive equations discretized on a C-grid [Arakawa and Lamb, 1977] using the classical Boussinesq and rigid lid approximations. The horizontal mesh is curvilinear and orthogonal, which ensures a second order numerical accuracy [Marti et al., 1992]. The grid is distorted in the northern hemisphere so that the northern singularity is shifted to be over Asia. Horizontal grid spacing varies between  $0.5^\circ$  and  $2^\circ$  with its higher meridional resolution in the equatorial regions as a means to better resolve fine-scale features important in equatorial dynamics. The model has 30 vertical levels among which 10 are located in the top 100 m. The model is driven with monthly mean climatologies of wind stress [Hellerman and Rosenstein, 1983]. Heat fluxes and water fluxes are from Oberhüber [1988]. Additionally, surface salinity and surface temperature are restored toward climatological values [Levitus, 1982] using a damping time constant of 12 days.

Effects of non-resolved sub-grid-scale movements on the large-scale circulation are parameterized by horizontal and vertical eddy diffusivities and viscosities. The horizontal eddy viscosity coefficient is imposed by the resolution. It is set to be equal to  $4 \times 10^4 \text{ m}^2 \text{ s}^{-1}$

everywhere, except between  $20^{\circ}\text{S}$  and  $20^{\circ}\text{N}$  where it is gradually reduced to attain  $2000 \text{ m}^2\text{s}^{-1}$  at the equator. This reduction accounts for the ratio between the typical scale of the eddies and the horizontal spacing which is smaller when near the equator than in higher latitudes. The horizontal eddy diffusivity coefficient is constant everywhere at  $2000 \text{ m}^2\text{s}^{-1}$ . Vertical eddy diffusivity is not defined a priori. Instead, OPA includes a prognostic model of the turbulence based on the equations of the turbulent kinetic energy (TKE) proposed by Gaspar et al. [1990] and adapted to OPA by Blanke and Delecluse [1993]. Thus, OPA predicts turbulence and computes vertical eddy diffusivity and viscosity coefficients throughout the water column, i.e. within the mixed layer as well as below.

Because of OPA's relatively high horizontal and vertical resolution, it is run in a semi-diagnostic mode: temperature and salinity are restored toward the climatological values of Levitus [1982] throughout most of the ocean. The restoring time constant used varies with depth from 50 days at 15 m (level 2 of OPA) to 1 yr in the deep ocean. This approach is conceptually similar to the technique used by Toggweiler et al. [1989] in their "robust-diagnostic" version of the GFDL model. Practically though there are major differences. In OPA, restoration of temperature and salinity is relaxed in four areas: (1) in the mixed layer (which is thus predicted prognostically), (2) in the equatorial regions where small errors in observed density would lead to large errors in model-predicted velocity fields [Fujio and Imasato, 1991], (3) in the high latitudes where measurements are rare and biased toward summer values, and (4) along ocean-land boundaries to allow the model to reconstruct its own boundary currents.

Here we have used a tracer transport (off-line) version of OPA developed by Marti [1992]. This model uses monthly mean fields of advection, turbulence, temperature and salinity as predicted by the on-line model. Advective transport of tracers is computed according to the MPDATA scheme of Smolarkiewicz [1982], Smolarkiewicz [1983] and Smolarkiewicz and Clark [1986]. Although expensive, this scheme is little diffusive and positive definite (i.e., it avoids negative tracer concentrations).



## 2.2. Carbon-cycle model

The biogeochemical model coupled to OPA is HAMOCC3 [Maier-Reimer, 1993]. Our first priority was to keep HAMOCC3 in its original state in order to allow a rigorous comparison of our results with results with those from Maier-Reimer [1993]. Although some minor adaptations were necessary, their effect is negligible as discussed below.

For more efficient use with OPA, we adapted HAMOCC3 to include only 7 prognostic tracers, instead of the 20. We kept only those tracers necessary for the computation of the different biogenic fluxes of carbon: DIC, alkalinity,  $O_2$ , calcite,  $PO_4^{3-}$ , particulate organic carbon (POC), and  $SiO_2$ . These fluxes are divided into two components: the soft tissue pump and the hard tissue counterpump. The soft-tissue pump is reduced, in the model, to the export production (EP), defined simply as the part of the primary production transported out of the euphotic zone. EP is computed using following equation:

$$EP = r_0 I \frac{50}{Z_m} \frac{T + 2}{T + 10} \left( \frac{[PO_4^{3-}]}{[PO_4^{3-}] + P_0} \right) [PO_4^{3-}] \quad (1)$$

where  $r_0$  is the maximum productivity rate,  $I$  is the incoming radiation,  $Z_m$  is the mixed layer depth,  $T$  is the temperature (Celsius), and  $P_0$  equals  $0.02 \mu\text{mol P/l}$ . Export production is reduced in nutrient-poor water by a simple Michaelis-Menten kinetics formula which depends on the local concentration of  $PO_4^{3-}$  [Dugdale, 1967]. In HAMOCC3,  $PO_4^{3-}$  is chosen as the limiting nutrient to avoid complexities associated with nitrogen cycling. The thickness of the euphotic zone is set to 50 m globally. The maximum production efficiency  $r_0$  is set to 0.25/month as chosen by Maier-Reimer [1993] to adjust his model output to fit the surface observed phosphate distribution. The significance of the chosen value for  $r_0$  is that at most 25% of local  $PO_4^{3-}$  can be removed each month from the surface by the biological activity. The intensity of the hard-tissue counter-pump is deduced from export production via the rain ratio (Organic C/ $CaCO_3$  ratio) [Broecker and Peng, 1982]. This ratio depends on temperature and the local concentration of silicate. Its maximum value is set in HAMOCC3 to 0.35.

POC produced in the euphotic zone is exported instantaneously to 100 m, below which it is remineralized according to a power law function proportional to  $z^{-0.8}$  [Berger et al., 1987]. In HAMOCC3, denitrification is not considered. Thus, the remineralization of the organic matter is restricted to regions with sufficient oxygen ( $\leq 1 \mu\text{mol L}^{-1}$ ).

Otherwise, POC is preserved and transported by advection and diffusion. Exponential functions are prescribed to predict the export of calcareous shells and opal. Calcite dissolves with respect to the degree of saturation of seawater.

At the sea surface, the ocean exchanges  $\text{CO}_2$  and  $\text{O}_2$  with the atmosphere. The net flux from air to sea  $F$  is proportional to the difference between the partial pressure of the gas in the air  $P_a$  and the partial pressure at the sea surface  $P_s$ :

$$F = k\alpha(P_a - P_s) \quad (2)$$

where  $k$  is the gas transfer velocity (in  $\text{m s}^{-1}$ ),  $\alpha$  is the gas solubility ( $\text{mol m}^{-3} \mu\text{atm}^{-1}$ ). Instead of using a constant coefficient as did Maier-Reimer [1993], we computed the piston velocity by using eq. (8) from Wanninkhof [1992], a quadratic function of wind speed that includes a chemical enhancement at low wind speeds. For the latter, we used climatological mean values (Boutin and Etcheto, personal communication). The resulting global mean  $K$  ( $K=k\alpha$ ) has been corrected so that it equals the value of  $0.06 \text{ mol m}^{-2} \mu\text{atm}^{-1} \text{ yr}^{-1}$  deduced from  $^{14}\text{C}$  observations [Broecker et al., 1985].

### 2.3. Initial conditions and model integration

Simulations are initialized with uniform distributions of tracers.  $\text{PO}_4^{3-}$  concentration is set to  $2.1 \mu\text{mol L}^{-1}$ , the observed global mean computed from Conkright et al. [1994]. Dissolved inorganic carbon is set to be  $2350 \mu\text{mol L}^{-1}$ . Total alkalinity is initialized to  $2374 \mu\text{eq kg}^{-1}$  [Takahashi et al., 1981]. Preindustrial atmospheric  $\text{pCO}_2$  is fixed at 278 ppm.

A final steady-state is reached when globally and annually averaged air-to-sea flux of  $\text{CO}_2$  is zero. Since in theory this would require an infinitely long integration, we chose a small threshold value below which the model was considered to be at equilibrium. We used our recently developed technique DEGINT to reach equilibrium more rapidly [Aumont et al., 1997]; steady-state simulations were accelerated by a factor of 20. At equilibrium, the model's annual global mean air-to-sea  $\text{CO}_2$  flux integrated is  $0.05 \text{ GtC/yr}$ .

### 3. Results

#### 3.1. The simulated equatorial Pacific dynamics

Intense currents of limited meridional extent characterize equatorial dynamics in the Pacific. OPA's enhanced meridional resolution in this region suggests that it should better simulate equatorial dynamics relative to other coarse-resolution global models. Below we discuss the main dynamic features of OPA that play a role in controlling the distribution of the biogeochemical tracers.

Figure 1 shows a section of the zonal velocity field along  $150^\circ\text{W}$ . This section reveals that equatorial currents in OPA compare reasonably well with the observations Wyrтки and Kilonsky [1984]. In particular, OPA is able to simulate a vigorous equatorial undercurrent (EUC) centered at the Equator, whose speed exceeds  $1 \text{ m s}^{-1}$ . The model maximum speed of  $1.4 \text{ m s}^{-1}$  at  $140^\circ\text{W}$  is close to that observed ( $1.6 \text{ m s}^{-1}$ ) [Qiao and Weisberg, 1997]. Below the EUC, observations [Wyrтки and Kilonsky, 1984] show the presence of a geostrophic westward current, the equatorial intermediate current (EIC), whose speed can reach  $0.15 \text{ m s}^{-1}$ . The model does not clearly reproduce the EIC. However, we know of no model that is able to reproduce such a current on an annual mean. OPA simulates a stronger EIC during boreal summer. In August, simulated speeds reach  $0.13 \text{ m s}^{-1}$  at  $150^\circ\text{W}$  and at a depth of about 500 m. The intensity of this short-lived current in the model is of roughly the same magnitude as offered by Wyrтки and Kilonsky [1984] as the annual mean.

At the surface, the south equatorial current (SEC), flowing westward, presents two distinct maxima: one north and one south of the equator (Figure 2). The SEC's double maximum is due to frictional effects of the EUC which flows in the opposite direction and splits the SEC below the surface. The SEC is limited to the surface 200 m and is more rapid in the north. North of the SEC, the north equatorial countercurrent (NECC) flows eastward between  $4^\circ\text{N}$  and  $10^\circ\text{N}$ . Coarse resolution models generally fail to reproduce the NECC because of their insufficient horizontal resolution [Winguth et al., 1994]. In OPA, the core of the NECC is located in subsurface, between 60 m and 100 m as observed [Wyrтки and Kilonsky, 1984]. However OPA's maximum speed  $0.25 \text{ m s}^{-1}$  is too slow relative to the observed value of  $0.4 \text{ m s}^{-1}$ . North of the NECC, the model generates the

strong north equatorial current (NEC). Figure 2 shows that the surface zonal current simulated by OPA compares well with the drifter-derived climatology of Reverdin et al. [1994] although the NECC is too weak.

Figure 3 represents the vertical velocity in the Pacific equatorial region. The winds blowing westward create a divergence at the equator. Consequently sub-surface water is upwelled to the surface. Simulated vertical speeds are maximum in the central Pacific between  $110^{\circ}\text{W}$  and  $140^{\circ}\text{W}$  in a narrow meridional band spanning  $1^{\circ}$ . Vertical upwelling decreases as one moves eastward towards Central America. Maximum upward velocities in the model attain  $35 \times 10^{-6} \text{ m s}^{-1}$  whereas observed values exceed  $50 \times 10^{-6} \text{ m s}^{-1}$  [Poulain, 1993]. The associated vertical transport equals 38.6 Sv at 50 m for the area within  $170^{\circ}\text{E}$  to  $100^{\circ}\text{W}$  and  $5^{\circ}\text{S}$  to  $5^{\circ}\text{N}$ . Observed values range from 37-51 Sv [Wyrtki, 1981]. The equatorial divergence in OPA exhibits large seasonal variability with distinct maxima in April-May and October-November, as in the observations [Poulain, 1993]. Along the Peruvian coast, northward wind stress forces coastal upwelling between  $2^{\circ}\text{S}$  and  $15^{\circ}\text{S}$ . In this area, OPA transports 3.8 Sv upward toward the surface in agreement with the observed 4 Sv [Wyrtki, 1963].

To help diagnose tracer distributions in the equatorial Pacific, we determined the model's annual mean water transport budget for the upper eastern Pacific ocean. This region is exactly where coarse-resolution models develop nutrient trapping [Najjar et al., 1992; Maier-Reimer, 1993]. Laterally the region is defined as that between  $130^{\circ}\text{W}$  and  $80^{\circ}\text{W}$  and between  $5^{\circ}\text{S}$  and  $5^{\circ}\text{N}$ . Vertically, we further divided this region into three zones (Figure 4(a)): (1) the surface euphotic zone located in the top 50 m, (2) the intermediate zone between 50 m and 423 m which is affected by the EUC, and (3) the deep zone (423-870 m) where nutrient trapping is at its maximum. The equatorial divergence upwells 23.1 Sv of mid-depth waters into the productive surface zone. More than half of that is transported westward by the SEC out of the region defined above; the rest escapes meridionally.

The divergence is fed by water from the core of the EUC, which itself advects 33.3 Sv into the domain. The water flux at  $130^{\circ}\text{W}$  is substantially less (25.1 Sv) because in that region, the mid-depth box also includes the lower part of the westward flowing SEC. At  $80^{\circ}\text{W}$ , the EUC nearly vanishes due to continuous upwelling and subsequent

poleward divergence near the surface. The meridional geostrophic loss of water is small (1.1 Sv). Across the EUC, there is no input of water from the deep ocean. The deepest box correspond to the domain which should be affected by the EIC. Associated transport is 1.5 Sv, about one order of magnitude too small relative to annual mean estimates of Wyrski and Kilonsky [1984].

### 3.2. Simulated $\text{PO}_4^{3-}$

Figure 5 shows the annually averaged distribution of surface  $\text{PO}_4^{3-}$  as taken from the top 15 m layer in NODC world atlas [Conkright et al., 1994] and the top 10 m simulated by OPA. Maximum simulated  $\text{PO}_4^{3-}$  concentrations are found in the Peruvian upwelling where they exceed  $1 \mu\text{mol L}^{-1}$ , in agreement with the observations. Upwelled waters are transported northward and westward. Due to the westward transport, both in the model and observations, the Peruvian upwelling seems to feed the divergence with substantial  $\text{PO}_4^{3-}$ . However, it requires about 10 months for the water to move from the Peruvian coast to where the divergence is at its maximum ( $120^\circ\text{W}$ ), as determined from the modeled zonal velocity of  $10 \text{ cm s}^{-1}$  in this region. Thus most of the upwelled  $\text{PO}_4^{3-}$  is consumed in the model by the biology before it reaches the divergence, because in that region modeled production efficiency is at its maximum (0.25/month). Further west of coastal upwelling, at  $105^\circ\text{W}$ , the model simulates a second maximum. Also located there is the model's local maximum in vertical velocity.

Both modeled and observed distributions of  $\text{PO}_4^{3-}$  are asymmetrical with respect to the equator. East of  $150^\circ\text{W}$ , maximum surface concentrations are located mainly in the southern hemisphere. Lower values in the northern hemisphere are due to the NECC, bringing in waters with lower  $\text{PO}_4^{3-}$  concentrations from the western Pacific, where it originates.

Figures 6(a) and 6(b) show sections of observed  $\text{PO}_4^{3-}$  and modeled total phosphorus concentrations along the equator in the Pacific ocean. In the model, we consider total phosphorus ( $\text{PO}_4^{3-} + \text{POC}$ ) because the model's lack of oxygen in the eastern Pacific ocean produces a large pool of unremneralized POC (see Figures 14(a) and 14(b) in Maier-Reimer [1993]). Total P could be defined as that P which is potentially available for biological consumption. Considering previous modeling efforts, it is remarkable that

OPA-HAMOCC3 exhibits only a minor case of nutrient trapping. At 800 m, the model's maximum concentration is  $3.5 \mu\text{mol L}^{-1}$ , about  $0.5 \mu\text{mol L}^{-1}$  higher than in the observations. In comparison, the difference between modeled and observed concentrations exceeds  $2.5 \mu\text{mol L}^{-1}$  in Maier-Reimer [1993] and  $1.5 \mu\text{mol L}^{-1}$  in Najjar et al. [1992] at about the same depth. Since we use the same biogeochemical model as Maier-Reimer [1993], the improvement must be due to the different modeled circulation, particularly the different equatorial dynamics. Causes of the improvement are examined below.

On its way westward, the EUC is progressively enriched in  $\text{PO}_4^{3-}$  due to export production from above. Originating in the far western Pacific ocean, the EUC advects water having lower  $\text{PO}_4^{3-}$  concentrations into waters enriched in  $\text{PO}_4^{3-}$ . Thus, the EUC dilutes mid-depth waters that are brought to the surface by the divergence. As a consequence, the undercurrent is largely responsible for the sharp vertical gradient between 50 m and 400 m. The model's vertical gradient is weaker than observed, in part because the simulated EUC extends too deeply, i.e., there is no EIC (see section 3.1). The model's poorly constrained remineralization scheme may also be somewhat responsible.

### 3.3. $\text{PO}_4^{3-}$ budget

To better understand why OPA exhibits little nutrient trapping, we constructed a phosphorus budget for the eastern equatorial Pacific (Figure 7(a)), dividing the region into the same 3 vertical layers as for the water mass budget (Figure 4). The EUC's role in this budget seems a paradox. On one hand, the EUC is the major supplier of water and nutrients, advecting  $34.3 \text{ kmol P s}^{-1}$  into the eastern Pacific; on the other hand, the EUC dilutes nutrient concentrations because its source is in the west where  $\text{PO}_4^{3-}$  concentration are on average  $0.6 \mu\text{mol L}^{-1}$  lower than in the richer waters upwelled toward the surface.

Of the  $42.1 \text{ kmol P s}^{-1}$  brought into the intermediate box by the EUC and export production from above,  $3/4$  is upwelled into the productive zone. The remaining  $1/4$  is advected latitudinally; 75% of that is lost by transport to the south. Some of this southward outflow eventually feeds into the Peru upwelling. Such is consistent with observations that indicate that waters upwelled off the coast of Peru originate from the lower part of the EUC [Wyrski, 1963; Lukas, 1986; Toggweiler et al., 1991].



In the euphotic zone, about 2/3 of the  $\text{PO}_4^{3-}$  upwelled from the mid-layer box exit the surface box laterally. Lateral loss is divided nearly equally between transport by the westward flowing SEC and meridional transport across the southern and northern edges. Toggweiler and Carson [1995] found a somewhat lower amount, about 50%, leaving the surface box by lateral export, after summing transport of nitrate (30%) and organic matter (20%). Concerning the remaining 1/3 of the phosphorus which leaves the euphotic zone in OPA-HAMOCC3, it is exported into deeper layers by sinking particles. Observed export production Murray et al. [1994] is  $2.5 \text{ mmol C m}^{-2} \text{ d}^{-1}$  at 120 m along  $140^\circ\text{W}$ . At the same depth and location, modeled export production is  $2.33 \text{ mmol C m}^{-2} \text{ d}^{-1}$ .

Fluxes into and out of the deep box are much smaller. In OPA, there is little input of phosphorus from the deep ocean. None of that makes it across OPA's strong EUC. Such minimal upwelling is remarkable for coarse-resolution global models but not for high-resolution regional models [Toggweiler and Carson, 1995]. This lack of upwelled deep phosphorus was expected in view of the water mass budget. Phosphorus entering the deep box by transport or export production leaves it through the deep-box's western limit.

Observational and modeling studies [Tsuchiya, 1981; Toggweiler et al., 1991; Blanke and Raynaud, 1997] have shown that most of the water entering into the equatorial Pacific's source zone for the EUC, derives from the Southern Hemisphere. To better determine its source in OPA, we analyzed nutrient transport in the area comprised between  $5^\circ\text{S}$  and  $5^\circ\text{N}$  and  $130^\circ\text{E}$  and  $150^\circ\text{E}$  (not shown) where the EUC originates. We found that of the  $16 \text{ kmol P}$  entering that box every second, roughly 70% derives from the Southern Hemisphere, mostly transported by the New Guinea Undercurrent (NGUC).

### 3.4. Sensitivity tests

OPA has two peculiarities which have potential to contribute to its improved ability to match observed phosphate. First, OPA's  $0.5^\circ$  meridional resolution near the equator is enhanced relative to the roughly  $4^\circ$  resolution used by other global scale coarse-resolution models. Second is OPA's prognostic parameterization of vertical turbulence, throughout the water column. A third difference, OPA's semi-diagnostic forcing, does not play a role because OPA is completely prognostic in the equatorial region. The combined higher

resolution and TKE model of vertical turbulence are together responsible for the absence of substantial nutrient trapping. To determine the contribution of each, we performed two sensitivity tests with the online version of OPA.

For the first test, we increased the equatorial horizontal viscosity coefficients used in OPA ( $2000 \text{ m}^2 \text{ s}^{-1}$ ) by a factor of twenty to their extra-tropical value ( $40000 \text{ m}^2 \text{ s}^{-1}$ ). We term this as case HV. Such an experiment is motivated by the use of large horizontal eddy viscosity coefficients in coarse-resolution models, as required to avoid numerical problems (i.e., to simulate smooth solutions). Due to such high viscosity, simulated horizontal speeds in coarse-resolution models are often underestimated, particularly the speed of the EUC [Toggweiler et al., 1989]. However, our case HV is not exactly equivalent to a decrease of the resolution. Much poorer resolution alters equatorial dynamics simply because the grid size is too large to correctly resolve, meridionally, the fine-scale equatorial currents such as the EUC or the NECC. Thus our case HV infers only some of the changes due to using a coarser resolution; a full coarse-resolution model would perform more poorly.

In the second sensitivity test, OPA was run without the prognostic parameterization of vertical turbulence. Instead, one vertical diffusion coefficient is defined a priori as equal to  $0.3 \text{ cm}^2 \text{ s}^{-2}$  everywhere within the ocean. We term this as case CVD. Both sensitivity tests were performed with the online version of OPA. Resulting monthly averaged dynamic fields were used to drive the offline version of the model, as in our standard run.

Figure 4 includes the water mass budgets for both sensitivity tests. In case HV, water fluxes exhibit two major differences relative to those from the standard case. First, the EUC is weaker, bringing in 29.5 Sv instead of 33.3 Sv for the standard case. A decrease in the intensity of the EUC was also found in a similar experiment by Maes et al. [1997]. This decrease is not apparent in the total mass transport between 50 m and 430 m because the deepest part of the westward flowing SEC is also slower in case HV. Secondly, in case HV, upwelling from the deep ocean (i.e., at the base of deep box) increases nine-fold, to 1.8 Sv. In case CVD, the most noticeable difference is the 36% increase in upwelling at 50 m. Such a result might be expected given the study by Blanke and Delecluse [1993] who show a 66% increase of the near-surface upwelling at the equator in a tropical Atlantic

version of OPA, when a more classical Richardson number based scheme is used instead of TKE to describe vertical turbulence. The TKE scheme predicts higher near-surface vertical mixing which deepens the Ekman layer, and increases the vertical dissipation. Thus, meridional velocities are slower leading to a weaker near-surface upwelling.

Figure 6 includes an equatorial section of total phosphorus for each of the two sensitivity runs. Case HV exhibits a substantial increase in nutrient trapping. For example, total phosphorus concentrations exceed  $4.4 \mu\text{mol L}^{-1}$  at 400 m along the American coast; in the standard run, total P concentrations reach at most  $3.7 \mu\text{mol L}^{-1}$ . Since the EUC is slower, waters within the EUC have longer to be enriched in nutrient from remineralization of sinking particles. As a consequence, mean phosphorus concentration in the intermediate box is  $0.34 \mu\text{mol L}^{-1}$  higher than in the standard case (Figure 7(b)). Case HV's P-enriched EUC causes P transport by that current to be 19% higher, despite the lower EUC intensity. Thus, waters upwelled to the surface in case HV have a much higher nutrient content. Resulting higher export production (+16%) and the larger inflow of nutrient-rich waters from the deep ocean explain increased nutrient trapping.

For case CVD, there is no increase in nutrient trapping. Surprisingly, maximum phosphorus concentrations ( $3.4 \mu\text{mol L}^{-1}$ ) are even lower than in the standard case ( $3.7 \mu\text{mol L}^{-1}$ ). Such a result is difficult to explain using the Najjar et al. [1992] analysis (Figure 8) which suggests that a more intense near-surface upwelling, such as found in this case, should increase nutrient trapping. The nutrient budget (Figure 7(c)) allows a better understanding. Although near-surface upwelling is greater, so is the intensity of the EUC. The EUC's increase in flow is modest at  $130^\circ\text{W}$  (about 5%) but at  $150^\circ\text{W}$ , closer to the source, the EUC is 12% stronger than in the standard case. As a consequence, the dilution induced by the EUC is stronger so that nutrient concentrations of the upwelled waters are about  $0.2 \mu\text{mol L}^{-1}$  lower than in the standard case. Thus, despite greater upwelling, export production remains almost unchanged (only a 3% increase). In the deepest box, the downwelling (0.5 Sv) of less nutrient rich water than in the standard case compensates the more than doubled inflow from the deep ocean.

## 4. Discussion

### 4.1. Nutrient trapping: the dynamic solution

Nutrient trapping is highly sensitive to the intensity of EUC. Decreased EUC flow in case HV results in a substantial increase of phosphorus below the divergence. Conversely, a slight increase of the intensity of the EUC in case CVD reduces nutrient trapping. Yet, the EUC acts indirectly because it lies above regions where nutrient trapping occurs. By advecting waters originating from the western part of the equatorial Pacific ocean, the EUC dilutes the nutrient-rich waters that are upwelled to the surface. By that manner, the EUC limits the intensity of export production and thus, the amount of nutrient released during remineralization in sub-surface waters. Coarse-resolution models are capable of producing only a weak EUC: a maximum speed of less than  $0.2 \text{ m s}^{-1}$  in the case of the GFDL model [Toggweiler et al., 1991] and of about  $0.5 \text{ m s}^{-1}$  in the case of the LSG model (Maier-Reimer, personal communication). A weak EUC results in higher  $\text{PO}_4^{3-}$  at the sea surface, higher export production, and higher remineralization. Models with weak EUC are thus obliged to generate the artefact known as nutrient trapping.

Nutrient trapping also results from excess upwelling of abyssal water into the upper equatorial Pacific. Our case HV shows that the rate of a model's abyssal upwelling is linked to its viscosity coefficients, which are tied to the model's chosen horizontal resolution. Coarse-resolution models that simulate nutrient trapping, produce excess upwelling of abyssal water to the surface tropical Pacific, roughly 4 Sv in the GFDL model [Toggweiler et al., 1991; Toggweiler and Samuels, 1993], and 10 Sv in the LSG model [Maier-Reimer et al., 1993]. Coral records of C-14 show that such upwelling is unrealistic [Toggweiler et al., 1991]. Excess upwelling of abyssal water directly influences nutrient trapping. When large amounts of nutrient-rich deep water are brought up to the surface equatorial Pacific ocean, export production is enhanced as is remineralization of  $\text{PO}_4^{3-}$ . Thus, deep upwelling of abyssal water causes additional organic matter to be exported to mid-depth waters, then reinjected once again into the divergence. Less nutrient is able to escape the system.

Both the weaker EUC and excess upwelling of abyssal water found in coarse-resolution models can be related to Najjar et al. [1992]'s analysis of nutrient trapping. They ex-

plain their 3-D model results in the context of a simple box model of the upper equatorial Pacific ocean (Figure 8(a)). Najjar et al. [1992] show that the nutrient concentration of the region from which upwelled water originates ( $N_a$ ) is a determining factor for nutrient trapping. The lower  $N_a$  is, the less nutrient trapping there is. Both a strong EUC and little or no upwelling of deep water are found in the real ocean and in OPA. Both factors lead to lower  $N_a$ . A higher  $N_a$  exists in coarse-resolution models because of their weak EUC and their large upwelling of abyssal water. Najjar et al. [1992] further point out that nutrient trapping increases with the proportion of organic matter remineralized within the divergence zone. In coarse-resolution models, that proportion is increased because additional organic matter is remineralized within the upwelled abyssal waters during their passage to the surface. That excess remineralization produces excess nutrient that is reinjected into the divergence zone. The same phenomenon would occur if the divergence zone extended too deeply in the model.

Another factor is the near-surface upwelling. In their simple box model, Najjar et al. [1992] show that a more intense near-surface upwelling  $u$  should increase nutrient trapping. In our case CVD, near surface upwelling increases but sub-surface nutrient build-up decreases. The reason is that in case CVD, the EUC is also more intense. For our simulations, where circulation is more realistic, near surface upwelling appears not to be a primary factor. We thus offer a slight revision to Najjar et al. [1992]'s box model, in which the EUC and the upwelling of abyssal waters are separated into two distinct processes (Figure 8(b)). As before,  $N_u$  declines as the intensity of the EUC ( $u_w$ ) increases and as deep upwelling ( $u_d$ ) decreases; near surface upwelling ( $u_s$ ) plays a little role.

#### 4.2. Implications for the carbon cycle

Observations show that DIC concentrations of surface waters in the equatorial Pacific ocean are about  $100 \mu\text{mol L}^{-1}$  lower than those of the upwelled waters. Such a drawdown is due to a combination of three processes: air-sea gas exchange, vertical export by sinking particles (POC), and formation and lateral export of DOC. The POC and DOC are of particular importance for the global carbon cycle because their formation results in a net sequestration of carbon in the ocean. However, the time scale for the ocean's sequestration of each varies enormously. A portion of the POC sinks below the thermocline.

That deep carbon remains in the ocean isolated from the atmosphere for centuries. On the other hand, DOC does not venture far from the surface; its lifetime is relatively quite short. Determining the partitioning between DOC and POC is critical to evaluating the natural capacity of equatorial Pacific to remove carbon from the surface of the ocean and thus from the atmosphere. That information is prerequisite to understanding how the DOC/POC ratio may be affected in future.

Controversy surrounds our understanding of the partitioning between DOC and POC. Until recently, horizontal export of carbon by DOC was thought to predominate in the equatorial Pacific (up to 75% of total export production) [Chavez and Barber, 1987; Murray et al., 1994; Feely et al., 1995]. The inability of global models to simulate realistic nutrient distributions unless they included DOC, concurred with such a paradigm [Najjar et al., 1992; Murray et al., 1994; Anderson and Sarmiento, 1995; Six and Maier-Reimer, 1996]. Thus, if DOC is so important, biological activity does not efficiently export carbon from the surface into the deep ocean in the equatorial Pacific. Most of the biologically removed carbon would then remain at the surface in the form of DOC and would be readily available for exchange with the atmosphere. Yet, a recent study disagrees. Using surface data for nutrients and for DIC, Hansell et al. [1997] find that DOC contributes at most 10% to the export of carbon. Accordingly, the other 90% or more must be lost by sinking particles and gas exchange. There seems a dilemma.

Modeling results presented here show that a realistic nutrient distribution can indeed be simulated both in surface and sub-surface waters with but a simple particle-only biogeochemical model. Absence of substantial nutrient trapping below the divergence indicates that OPA-HAMOCC3 does not overpredict vertical export by sinking particles. Such is confirmed by comparison between simulated and observed export production: OPA finds  $2.33 \text{ mmol C m}^{-2} \text{ d}^{-1}$ ; analysis of sediment trap data finds  $2.5 \text{ mmol C m}^{-2} \text{ d}^{-1}$  [Murray et al., 1994]. A POC-only model would overpredict nutrients if horizontal transport of DOC were the major process in the real ocean. Our results suggest that export of DOC does not play a dominant role in the carbon budget of the equatorial Pacific ocean. Thus in OPA, vertical export of POC ( $0.6 \text{ GtC/yr}$ ) represents 55% of the total DIC drawdown for the region between  $170^\circ\text{E}$  and  $80^\circ\text{W}$  and between  $5^\circ\text{S}$  and  $5^\circ\text{N}$ ; loss by air-sea exchange ( $0.48 \text{ GtC/yr}$ ) represents the remaining 45%. The measured results



from Hansell et al. [1997] are similar (53% by POC export; 41% by air-sea exchange).

The role played by DOC in the carbon budget of the equatorial Pacific seems to be quite inefficient. Observations show that its production is about  $8 \text{ mmol C m}^{-2} \text{ s}^{-1}$  [Feely et al., 1995], which is about 3 times higher than that of POC. Hence the reason why DOC is believed to be the major contributor to  $\text{CO}_2$  export. However, most of the DOC (about  $40 \text{ } \mu\text{mol L}^{-1}$ ) exists in a refractory form [Murray et al., 1994] whose mean lifetime is several thousand years [Williams and Druffel, 1987; Druffel et al., 1992]. That refractory DOC has a negligible impact on the carbon budget of this region.

There also exists a semilabile form of DOC found mostly within the top few hundred meters of the ocean. Lifetime of the semilabile DOC fraction has been estimated to be 30-120 days [Archer et al., 1997]. Given such a short lifetime, how far might the semilabile DOC be able to travel? In OPA, the upwelling rate is 38 Sv at 50 m for the region between  $5^\circ\text{S}$  to  $5^\circ\text{N}$  and  $100^\circ\text{W}$  to  $170^\circ\text{E}$ . The mean residence of waters in this region is about 170 days, which is at least 50% longer than mean lifetime of semilabile DOC. Thus, most semilabile DOC is remineralized before it has a chance to be advected out of the equatorial region.

Such a high turnover rate of about 2 months explains why observed DOC concentrations are increased by just  $10 \text{ } \mu\text{mol L}^{-1}$  between the equator and  $5^\circ$  [Archer et al., 1997]. A 38 Sv water outflux having  $10 \text{ } \mu\text{mol DOC L}^{-1}$  yields an export of about  $0.15 \text{ PgC yr}^{-1}$ . This is one fourth of OPA's export associated with sinking particles ( $0.6 \text{ GtC/yr}$ ). Our calculated DOC lateral export is slightly less than the  $0.2\text{-}0.4 \text{ PgC yr}^{-1}$  proposed by Archer et al. [1997] who used a model of the tropical Pacific which includes DOC. Adding this  $0.15 \text{ PgC yr}^{-1}$  export of DOC to the OPA-HAMOCC3 predicted  $1.08 \text{ PgC yr}^{-1}$  carbon loss ( $0.6 \text{ PgC yr}^{-1}$  as POC,  $0.48 \text{ PgC yr}^{-1}$  by air-sea exchange) leads to a total export of  $1.23 \text{ PgC yr}^{-1}$  out of the surface equatorial Pacific. According to this simple recipe, DOC contributes only 12% of total carbon export out of the equatorial Pacific ocean. This small contribution of DOC is similar to the 10Hansell et al. [1997]. Therefore, DOC seems to play a minor role in the carbon budget of the equatorial Pacific.

## 5. Conclusions

The OPA-HAMOCC3 model predicts phosphate concentrations in the subsurface equatorial Pacific which exceed the observed nutrient concentrations by at most 15 large excess nutrient concentrations (nutrient trapping) in this same region. OPA's improvement is due to its higher meridional resolution ( $0.5^\circ$  N-S) near the equator, which allows (1) a vigorous equatorial undercurrent (EUC) in the Pacific, as observed, and (2) a reduction of upwelling of abyssal water to the surface. Both effects reduce nutrient trapping. The EUC brings in low nutrient waters from the western Pacific, diluting concentrations in the east. Reduced abyssal upwelling cuts off the supply of nutrient-rich waters from below. Other global-scale carbon-cycle models have inadequate resolution to properly represent circulation features in the equatorial Pacific (such as the fine-scale EUC), which are prerequisites to getting the nutrient distribution right. Although previously suggested improvements to the biogeochemical model act to improve nutrient trapping, their necessity cannot be correctly evaluated until the circulation model does a proper job at representing equatorial dynamics. To avoid nutrient trapping, coarse-resolution models will have to employ higher meridional resolution at the equator. Our simulations with a coarser-resolution version of OPA [Braconnot et al., 1997] suggest that  $1^\circ$  meridional resolution is adequate.

We have shown that a realistic distribution of surface and subsurface  $\text{PO}_4^{3-}$  in the equatorial Pacific can be achieved in a model having only a particle-only remineralization scheme. These model results suggest that DOC does not play a dominant role in the carbon budget of the equatorial Pacific. According to our model-based calculations DOC accounts for only about 12% of the total carbon export out of the equatorial Pacific region. Recent observational constraints suggest that DOC is responsible for at most 10% the total carbon transport out of the same region Hansell et al. [1997].

**Acknowledgments.** Support for computations was provided by the CEA/DSM and by the CBRS/IDRIS. This work was funded by the Environment and Climate Programme of the European Community (contract ENV4-CT95-0132). We thank Ernst Maier-Reimer for providing us the biogeochemical model HAMOCC3.

## References

- Anderson, L. A. and J. L. Sarmiento, Global ocean phosphate and oxygen simulations, *Global Biogeochem. Cycles*, 9, 621–636, 1995.
- Andrich, P., OPA – A multitasked Ocean General Circulation Model, Reference manual, LODyC, Université Paris VI, Paris, FRANCE, 1988.
- Arakawa, A. and V. R. Lamb, Computational design of the UCLA general circulation model, *Methods Comput. Phys.*, 16, 173–283, 1977.
- Archer, D., E. T. Peltzer, and D. L. Kirchman, A timescale for dissolved organic carbon production in equatorial Pacific waters, *Global Biogeochem. Cycles*, 11, 435–452, 1997.
- Aumont, O., J. C. Orr, D. Jamous, P. Monfray, O. Marti, and G. Madec, A degradation approach to accelerate simulations to steady state in a 3-D tracer transport model of the global ocean, *Climate Dynamics*, in press, 1997.
- Bacastow, R. and E. Maier-Reimer, Ocean-circulation model of the Carbon cycle, *Clim. Dyn.*, 4, 95–125, 1990.
- Bacastow, R. and E. Maier-Reimer, Dissolved organic carbon in modeling oceanic new production, *Global Biogeochem. Cycles*, 5, 71–85, 1991.
- Berger, W. H., K. Fischer, C. Lai, and G. Wu, Ocean productivity and organic carbon flux, Part I, Overview of maps of primary production and export production, Sio ref. 87-30, Univ. of Calif., San Diego, 1987.
- Blanke, B. and P. Delecluse, Low frequency variability of the tropical Atlantic ocean simulated by a general circulation model with mixed layer physics, *J. of Phys. Oceanogr.*, 23, 1363–1388, 1993.
- Blanke, B. and S. Raynaud, Kinematics of the Pacific Equatorial Undercurrent: an Eulerian and Lagrangian approach from GCM results, *J. of Phys. Oceanogr.*, 27, 1038–1053, 1997.
- Braconnot, P., O. Marti, and S. Joussaume, Adjustment and feedbacks in a global coupled ocean-atmosphere model, *Clim. Dyn.*, 13, 507–519, 1997.
- Broecker, W. S. and T. H. Peng, *Tracers in the sea*, Eldigio, Palisades, 691pp, 1982.
- Broecker, W. S., T. S. Peng, G. Östlund, and M. Stuiver, The distribution of bomb radiocarbon in the ocean, *J. Geophys. Res.*, 90, 6953–6970, 1985.

- Chavez, F. P. and R. T. Barber, An estimate of new production in the Equatorial Pacific, *Deep Sea Res.*, 34, 1129–1243, 1987.
- Coale, K. H., K. S. Johnson, S. E. Fitzwater, R. M. Gordon, S. Tanner, F. P. Chavez, L. Ferioli, C. Sakamoto, P. Rogers, F. Millero, P. Steinberg, P. Nightingale, D. Cooper, W. P. Cochlan, M. R. Landry, J. Constantinou, G. Rollwagen, A. Trasvina, and R. Kudela, A massive phytoplankton bloom induced by an ecosystem-scale iron fertilization experiment in the equatorial Pacific Ocean, *Nature*, 383, 495–501, 1996.
- Conkright, M. E., S. Levitus, and T. P. Boyer, NOAA Atlas NESDIS 1: World ocean atlas 1994, vol. 1, Nutrients, Technical report, Natl. Oceanic and Atmos. Admin., Silver Spring, Md., 1994.
- Delecluse, P., M. Imbard, C. Lévy, and G. Madec, OPA-Ocean General Circulation model, Reference manual, LODYC, 1993.
- Druffel, E. R. M., P. M. Williams, J. E. Bauer, and J. R. Ertel, Cycling of dissolved and particulate organic matter in the open ocean, *J. Geophys. Res.*, 97, 15639–15659, 1992.
- Dugdale, R. C., Nutrient limitation in the sea: Dynamics, identification, and significance, *Limnol. and Oceanogr.*, 12, 685–695, 1967.
- Feely, R., A. R. Wanninkhof, C. E. Cosca, P. P. Murphy, M. F. Lamb, and M. D. Steckley, CO<sub>2</sub> distributions in the equatorial Pacific during the 1991-1992 ENSO event, *Deep Sea Res.*, 42, 365–386, 1995.
- Fujio, S. and N. N. Imasato, Diagnostic calculation for circulation and water mass movement in the deep Pacific, *J. Geophys. Res.*, 96, 759–774, 1991.
- Gammon, R. H., E. T. Sundquist, and P. J. Fraser, History of carbon dioxide in the atmosphere, *Atmospheric Carbon Dioxide and the Global Carbon Cycle*, 1985.
- Gaspar, P., Y. Gregoris, and J. M. Lefevre, A simple eddy-kinetic-energy model for simulations of the ocean vertical mixing: tests at station Papa and Long-Term Upper Ocean Study Site site, *J. Geophys. Res.*, 95, 1990.
- Guilyardi, E. and G. Madec, Performance of the OPA/ARPEGE-T21 global ocean atmosphere coupled model, *Climate Dyn.*, 13, 149–165, 1997.
- Hansell, D. A., N. R. Bates, and C. A. Carlson, Predominance of vertical loss of carbon from surface waters of the equatorial Pacific Ocean, *Nature*, 386, 59–61, 1997.

- Hellerman, S. and M. Rosenstein, Normal monthly wind stress over the world ocean with error estimates, *J. of Phys. Oceanogr.*, 13, 1093–1104, 1983.
- Levitus, S., Climatological atlas of the world ocean, NOAA Professional Paper 13, NOAA, Washington D.C., 1982.
- Lukas, R., The termination of the Equatorial Undercurrent in the Eastern Pacific, *Prog. Oceanogr.*, 16, 63–90, 1986.
- Madec, G. and M. Imbard, A global ocean mesh to overcome the North Pole singularity, *Clim. Dyn.*, 12, 381–388, 1996.
- Maes, C., G. Madec, and P. Delecluse, Sensitivity of an equatorial Pacific OGCM to the lateral diffusion, *Mon. Weather Rev.*, 125, 958–971, 1997.
- Maier-Reimer, E., Geochemical cycles in an ocean general circulation model: Preindustrial tracer distributions, *Global Biogeochem. Cycles*, 7(3), 645–677, 1993.
- Maier-Reimer, E., U. Mikolajewicz, and K. Hasselmann, Mean circulation of the Hamburg LSG OGCM and its sensitivity to the thermohaline surface forcing, *J. of Phys. Oceanogr.*, 23, 731–757, 1993.
- Marti, O., Etude de l'océan mondial: Modélisation de la circulation et du transport des traceurs anthropiques, Ph.D. thesis, Université Paris VI, Paris, FRANCE, 1992.
- Marti, O., G. Madec, and P. Delecluse, Comment on net "Net diffusivity in ocean general circulation models with non uniform grids", *J. Geophys. Res.*, 97, 12763–12766, 1992.
- Murray, J. W., R. T. Barber, M. R. Roman, M. P. Bacon, and R. A. Feely, Physical and biological controls on carbon cycling in the equatorial Pacific, *Science*, 266, 58–65, 1994.
- Najjar, R. G., Simulations of the phosphorus and oxygen cycles in the world ocean using a general circulatory model, Ph.D. thesis, Princeton Univ., Princeton, N.J., 1990.
- Najjar, R. G., J. L. Sarmiento, and J. R. Toggweiler, Downward transport and fate of organic matter in the ocean: Simulations with a general circulation model, *Global Biogeochem. Cycles*, 6, 45–76, 1992.
- Oberhuber, J. M., An atlas on the 'COADS' data set: The budget of heat, buoyancy, and turbulent kinetic energy at the surface of the global ocean, chapter 15, Max-Planck Institut für Meteorologie, 1988.

- Poulain, P. M., Estimates of horizontal divergence and vertical velocity in the equatorial Pacific, *J. of Phys. Oceanogr.*, 23, 601–607, 1993.
- Qiao, L. and R. H. Weisberg, The zonal momentum balance of the equatorial undercurrent in the central Pacific, *J. of Phys. Oceanogr.*, 27, 1094–1119, 1997.
- Reverdin, G., C. Frankignoul, E. Kestenare, and M. M. Phaden, A climatology of the seasonal currents in the equatorial Pacific, *J. Geophys. Res.*, 99, 20323–20344, 1994.
- Six, K. D. and E. Maier-Reimer, Effects of plankton dynamics on seasonal carbon fluxes in an ocean general circulation model, *Global Biogeochem. Cycles*, 10(4), 559–583, 1996.
- Smolarkiewicz, K. P., The multidimensional Crowley advection scheme, *Mon. Weather Rev.*, 110, 1968–1983, 1982.
- Smolarkiewicz, K. P., A simple positive advection scheme with small implicit diffusion, *Mon. Weather Rev.*, 111, 479–486, 1983.
- Smolarkiewicz, K. P. and T. L. Clark, The multidimensional positive definite advection transport algorithm: further development and applications, *J. of Comp. Phys.*, 67, 396–438, 1986.
- Sugimura, Y. and Y. Suzuki, A high-temperature catalytic oxidation method for the determination of non-volatile dissolved carbon in seawater by direct injection of a liquid sample, *Mar. Chem.*, 24, 105–131, 1988.
- Suzuki, Y., On the measurement of DOC and DON in seawater, *Mar. Chem.*, 41, 287–288, 1993.
- Suzuki, Y., Y. Sugimura, and T. Itoh, A catalytic oxidation method for the determination of total nitrogen dissolved in seawater, *Mar. Chem.*, 16, 83–97, 1985.
- Takahashi, T., W. S. Broecker, and A. E. Bainbridge, The alkalinity and total carbon dioxide concentration in the World Oceans, in *Carbon Cycle modeling in Scope*, edited by B. Bolin, pp. 271–286, John Wiley, New York, 1981.
- Toggweiler, J. R. and S. Carson, What are upwelling systems contributing to the ocean's carbon and nutrient budget, in *Upwelling in the ocean: Modern processes and ancient records*, edited by C. Summerhayes, K. Emeis, M. Angel, R. Smith, and B. Zeitzschel, pp. 337–360, John Wiley and Sons, Ltd., 1995.



- Toggweiler, J. R., K. Dixon, and W. S. Broecker, The Peru upwelling and the ventilation of the south Pacific thermocline, *J. Geophys. Res.*, 96, 20467–20497, 1991.
- Toggweiler, J. R., K. Dixon, and K. Bryan, Simulations of radiocarbon in a coarse-resolution world ocean model, 2, steady state pre-bomb distribution, *J. Geophys. Res.*, 94(C9), 8217–8242, 1989.
- Toggweiler, J. R. and B. Samuels, New radiocarbon constraints on the upwelling of abyssal water to the ocean's surface, in *The global carbon cycle*, edited by M. Heimann, volume I 15 of NATO ASI Series, pp. 333–366, Springer Verlag, Berlin Heidelberg, 1993.
- Tsuchiya, M., The origin of the Pacific Equatorial  $13^{\circ}\text{C}$  Water, *J. of Phys. Oceanogr.*, 11, 794–812, 1981.
- Wanninkhof, R., Relationship between wind speed and gas exchange over the ocean, *J. Geophys. Res.*, 97, 7373–7382, 1992.
- Williams, P. M. and E. R. M. Druffel, Radiocarbon in dissolved organic matter in the central Pacific Ocean, *Nature*, 330, 246–248, 1987.
- Winguth, A. M. E., M. Heimann, K. D. Kurz, E. Maier-Reimer, U. Mikolajewicz, and J. Segschneider, El-niño-Southern Oscillation related fluctuations of marine carbon cycle, *Global Biogeochem. Cycles*, 8, 39–63, 1994.
- Wong, C. S., Y. H. Chan, J. S. Page, G. E. Smith, and R. D. Bellegay, Changes in equatorial  $\text{CO}_2$  flux and new production estimated from  $\text{CO}_2$  and nutrients levels in Pacific surface waters during 1986/87 El Niño, *Tellus*, 45, 64–79, 1993.
- Wyrtki, K., The horizontal and vertical field of motion in the Peru current, *Bull. Scripps Inst. Oceanogr.*, 8, 313–346, 1963.
- Wyrtki, K., An estimate of equatorial upwelling in the Pacific, *J. of Phys. Oceanogr.*, 11, 1205–1214, 1981.
- Wyrtki, K. and B. Kilonsky, Mean water and current structure during the Hawaii-to- Tahiti shuttle experiments, *J. of Phys. Oceanogr.*, 14, 251–253, 1984.
- Yamanaka, Y. and E. Tajika, The role of the vertical fluxes of particulate organic matter and calcite in the oceanic carbon cycle: Studies using an ocean biogeochemical general circulation model, *Global Biogeochem. Cycles*, 10, 361–382, 1996.
-

O. Aumont, and J.C. Orr, Laboratoire de Modélisation du Climat et de l'Environnement, DSM, CE Saclay, CEA, L'Orme des Merisiers, Bât. 709, F-91191 Gif sur Yvette, Cedex, France

P. Monfray, Centre des Faibles Radioactivités, Laboratoire mixte CNRS-CEA, L'Orme des Merisiers, Bât. 709/LMCE, CE Saclay, F-91198 Gif sur Yvette, Cedex, France

G. Madec, Laboratoire d'Océanographie Dynamique et de Climatologie (CNRS/ORSTOM/UPMC), Université Paris VI, 4 place Jussieu, Paris, France

Received XXXXX ; revised XXXXXXXX; accepted XXXXX.

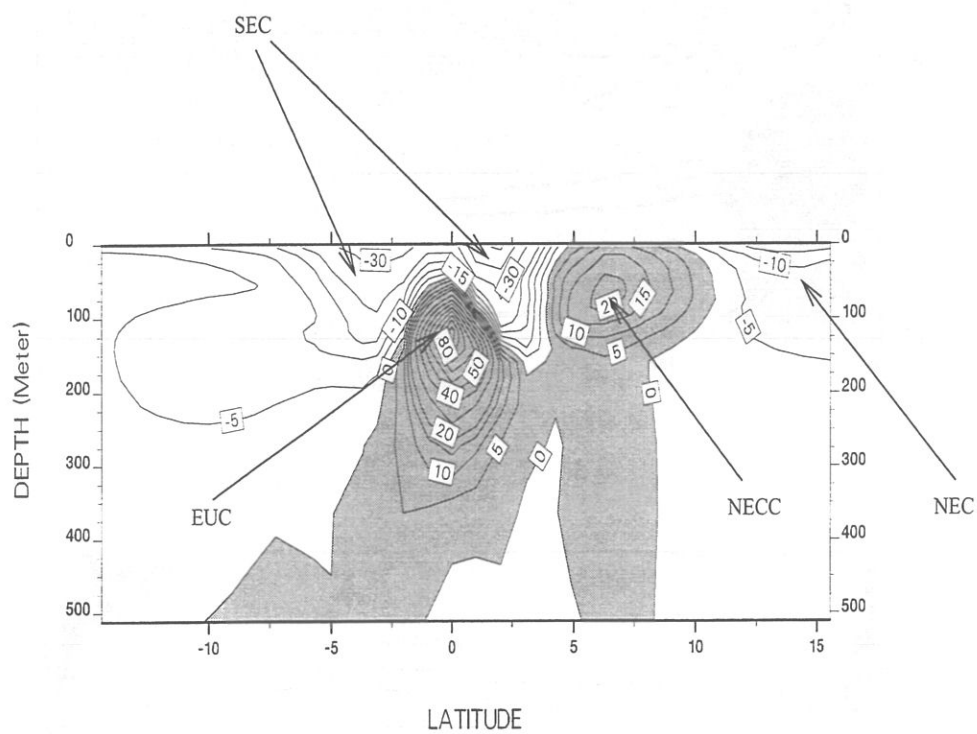
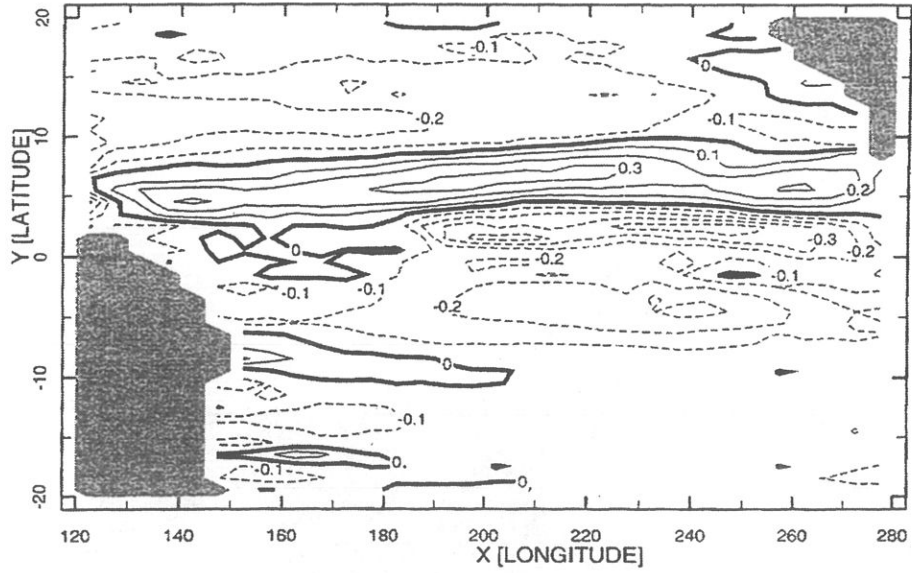


Figure 1. Annual mean distribution of zonal velocity speeds ( $\text{cm s}^{-1}$ ) simulated OPA along  $150^\circ\text{W}$  in the near surface. Positive speeds indicate eastward flow.

a)



b)

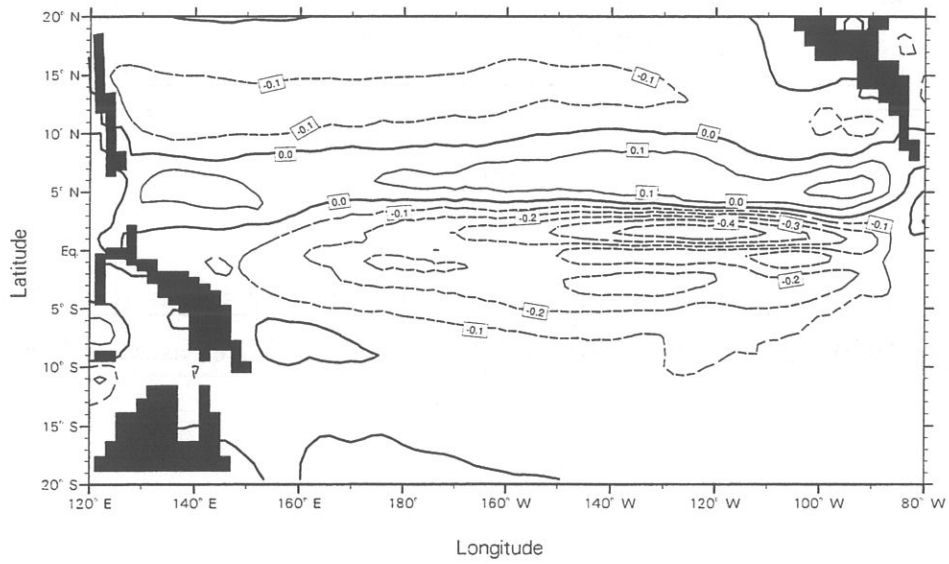


Figure 2. Annual mean distribution of zonal velocity speeds ( $\text{m s}^{-1}$ ) at 15 m (a) according to the drifter-derived climatology of Reverdin et al. [1994] (Figure from Rodgers et al. [1997]), and (b) in OPA.

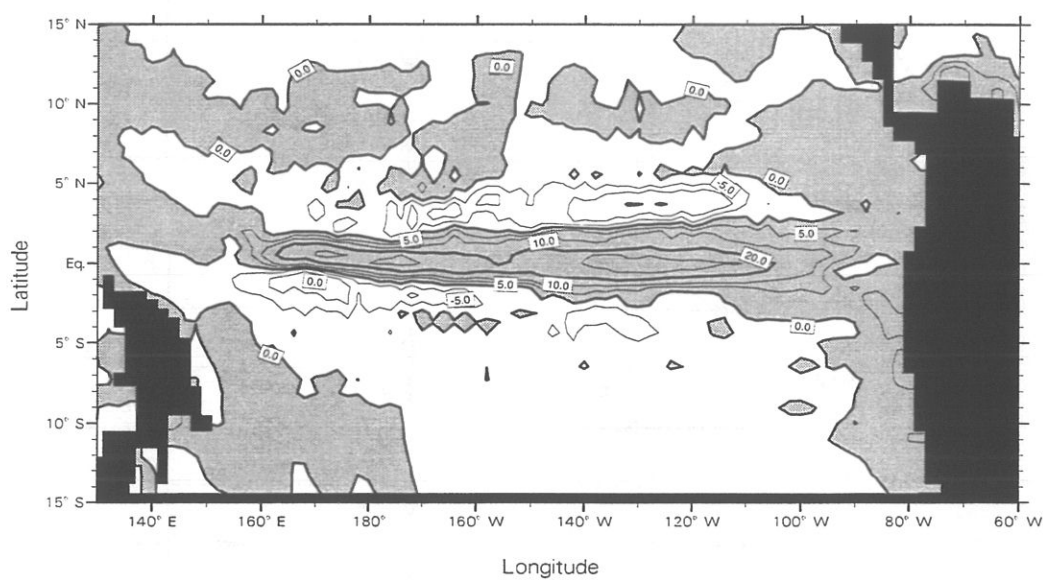


Figure 3. Modeled annual mean vertical velocity (in  $10^{-6} \text{ m s}^{-1}$ ) in the equatorial Pacific at 50 m. Contour levels are drawn at 0, 5, 10, 20, 30  $10^{-6} \text{ m s}^{-1}$ .

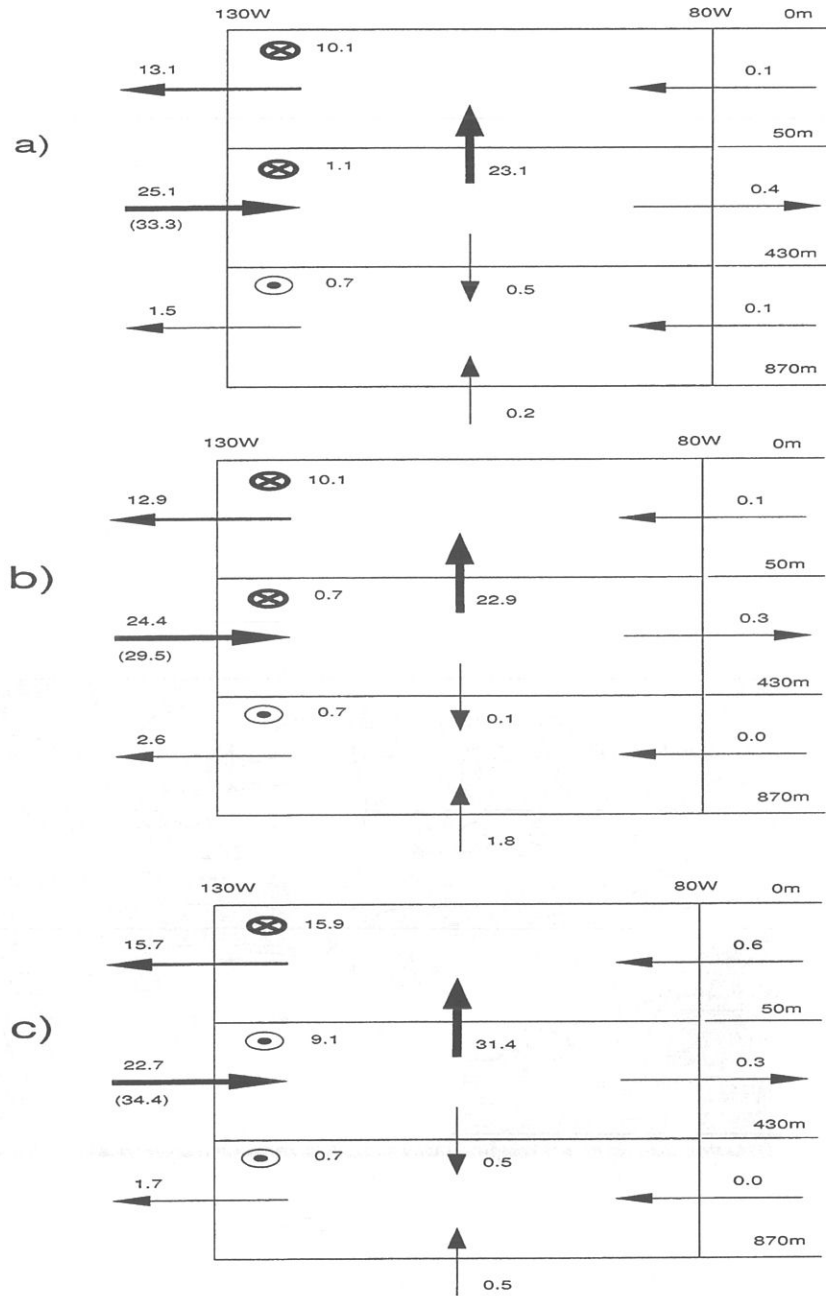


Figure 4. Water mass budget in the upper eastern equatorial Pacific ocean for OPA simulations: (a) standard case, (b) case HV, and (c) case CVD. Regions limits are 80°W–130°W, 4.7°S–4.7°N, and 0 m–870 m. Circled crosses indicate transport out of the domain; circled dots represent transport into the domain. The number in parentheses denotes the transport associated with the Equatorial Undercurrent only. All transports are in Sverdrup ( $1 \text{ Sv} = 10^{-6} \text{ m}^3 \text{ s}^{-1}$ ).



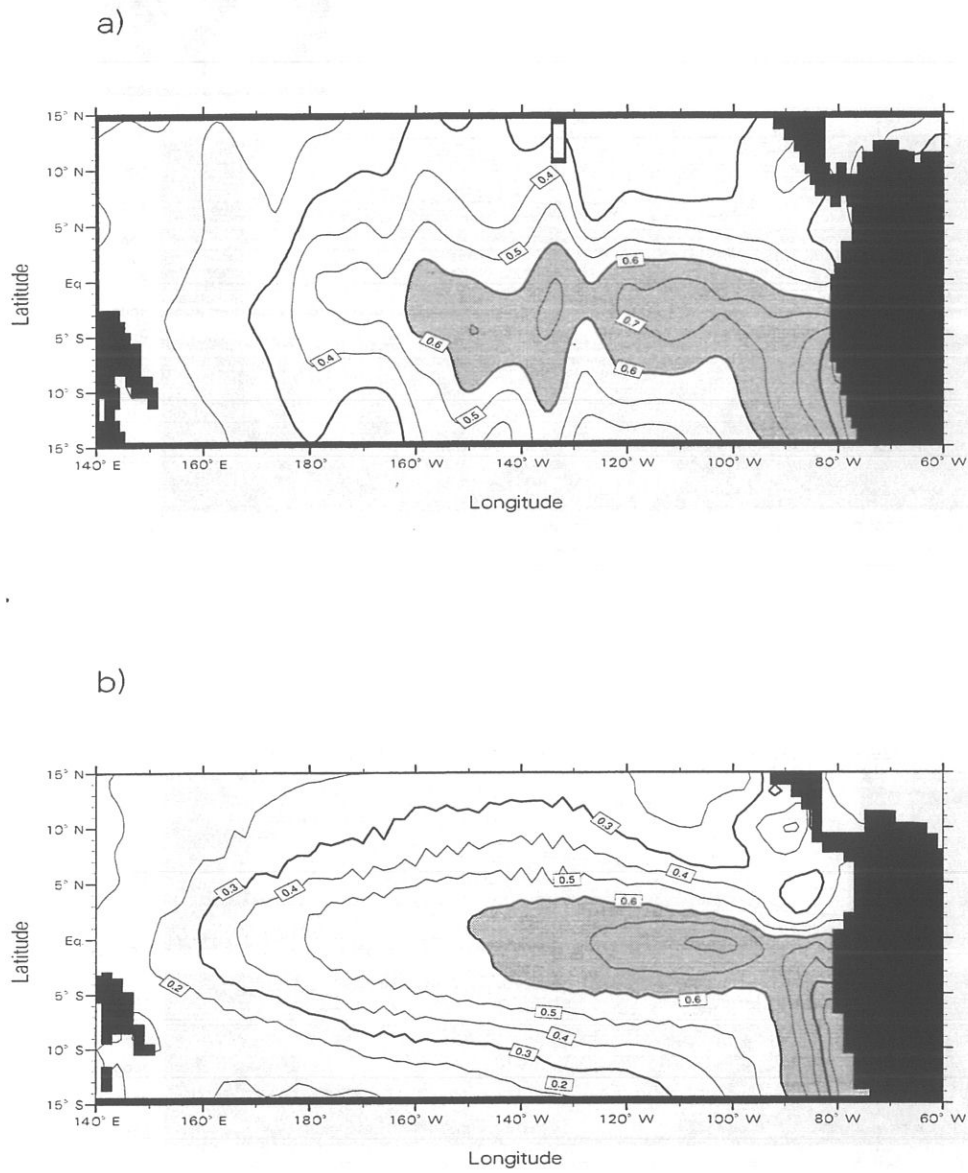


Figure 5. Annual mean distribution of  $\text{PO}_4^{3-}$  ( $\mu\text{mol L}^{-1}$ ) at sea surface in the equatorial Pacific: (a) observations from Conkright et al. [1994], and (b) output from OPA. Contours are given for every  $0.1 \mu\text{mol L}^{-1}$ .

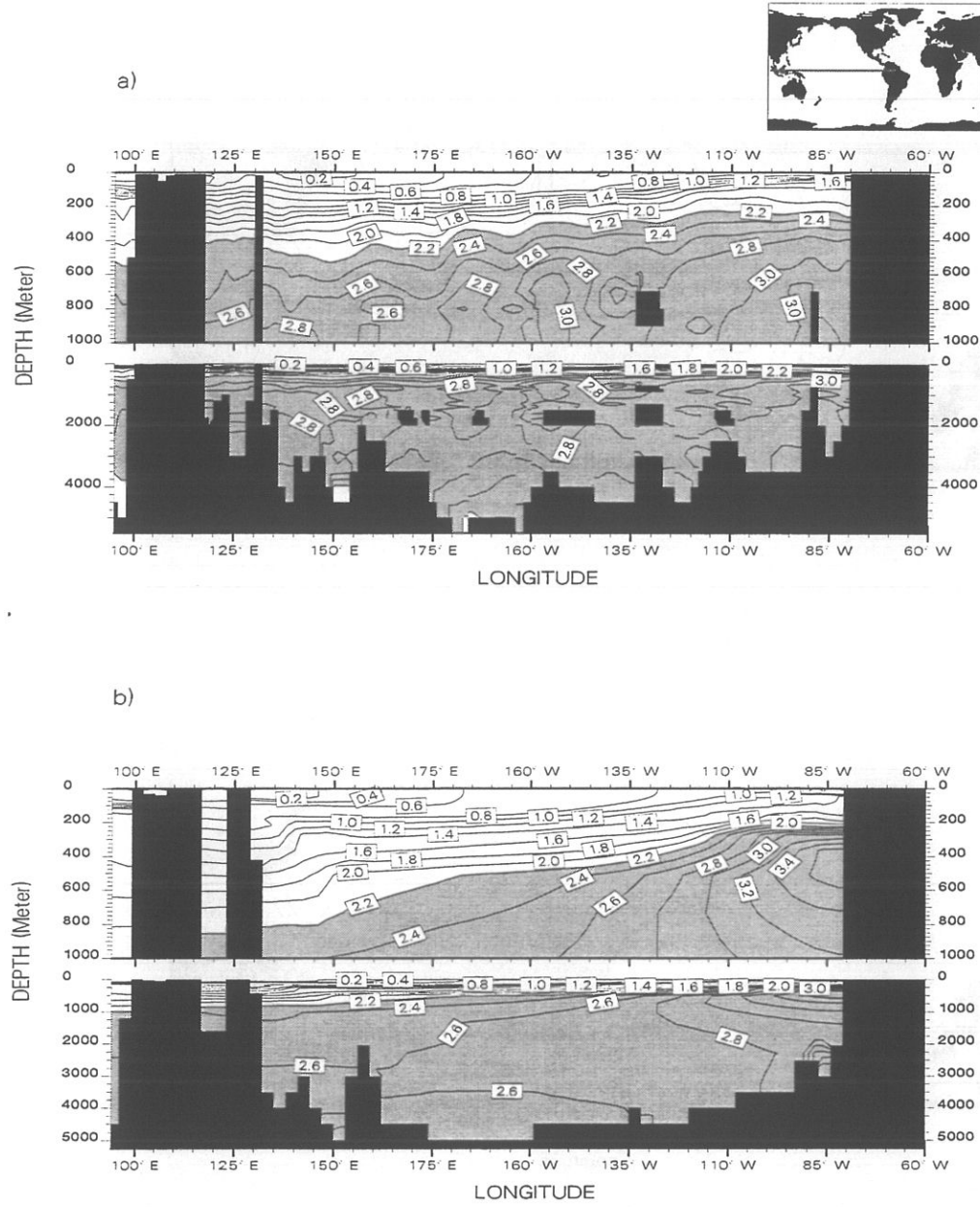


Figure 6.  $\text{PO}_4^{3-}$  distribution ( $\mu\text{mol L}^{-1}$ ) along the equator in the Pacific: (a) observations from Conkright et al. [1994], (b) standard case, (c) case HV, and (d) case CVD. For the model, total phosphorus is considered instead of  $\text{PO}_4^{3-}$  alone as explained in the text. Black areas in panel (a) correspond to the bathymetry but also to places where no data are available. The vertical scale of the upper 1000 m is displayed with expanded scale.

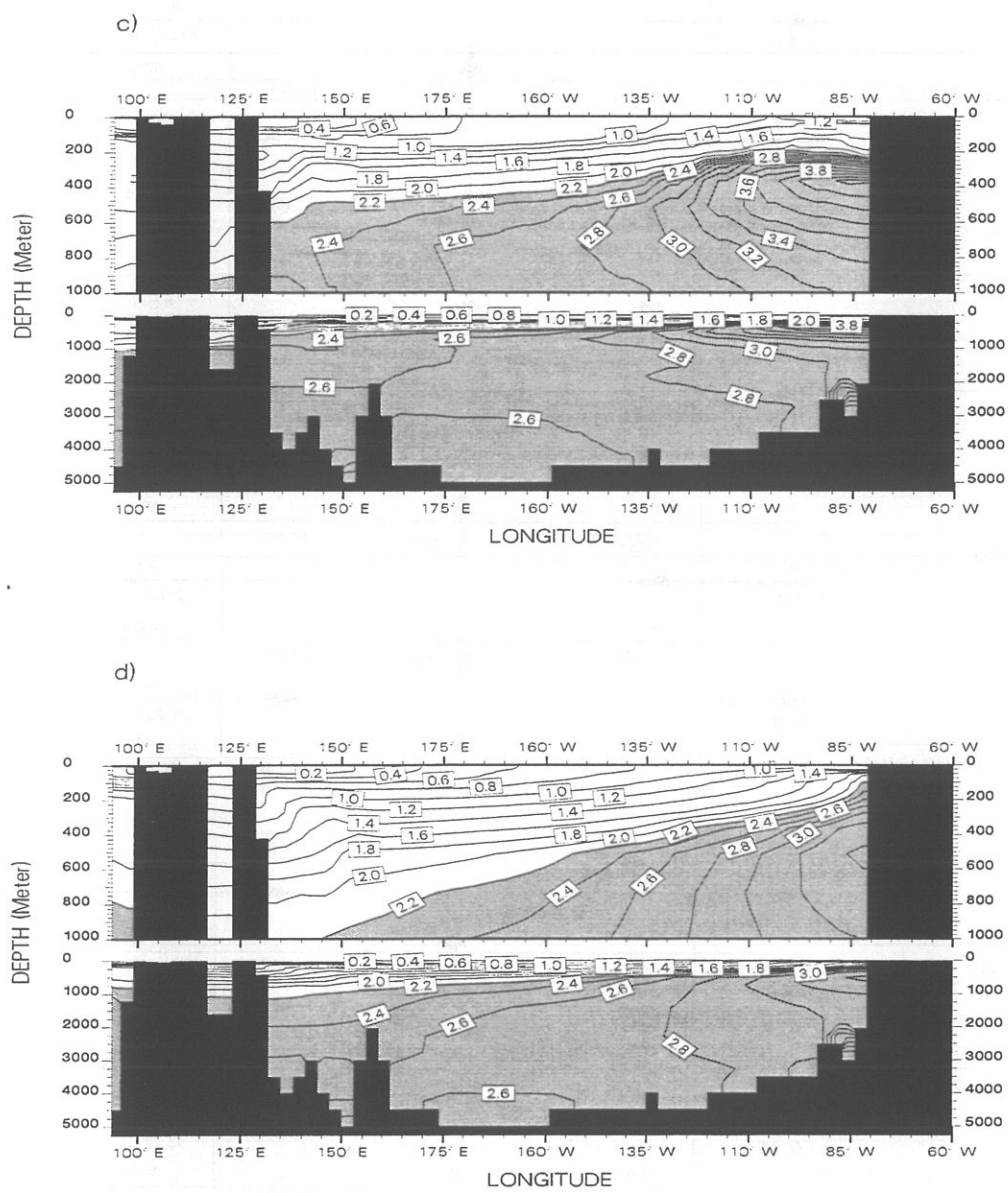


Figure 6. (Continued)

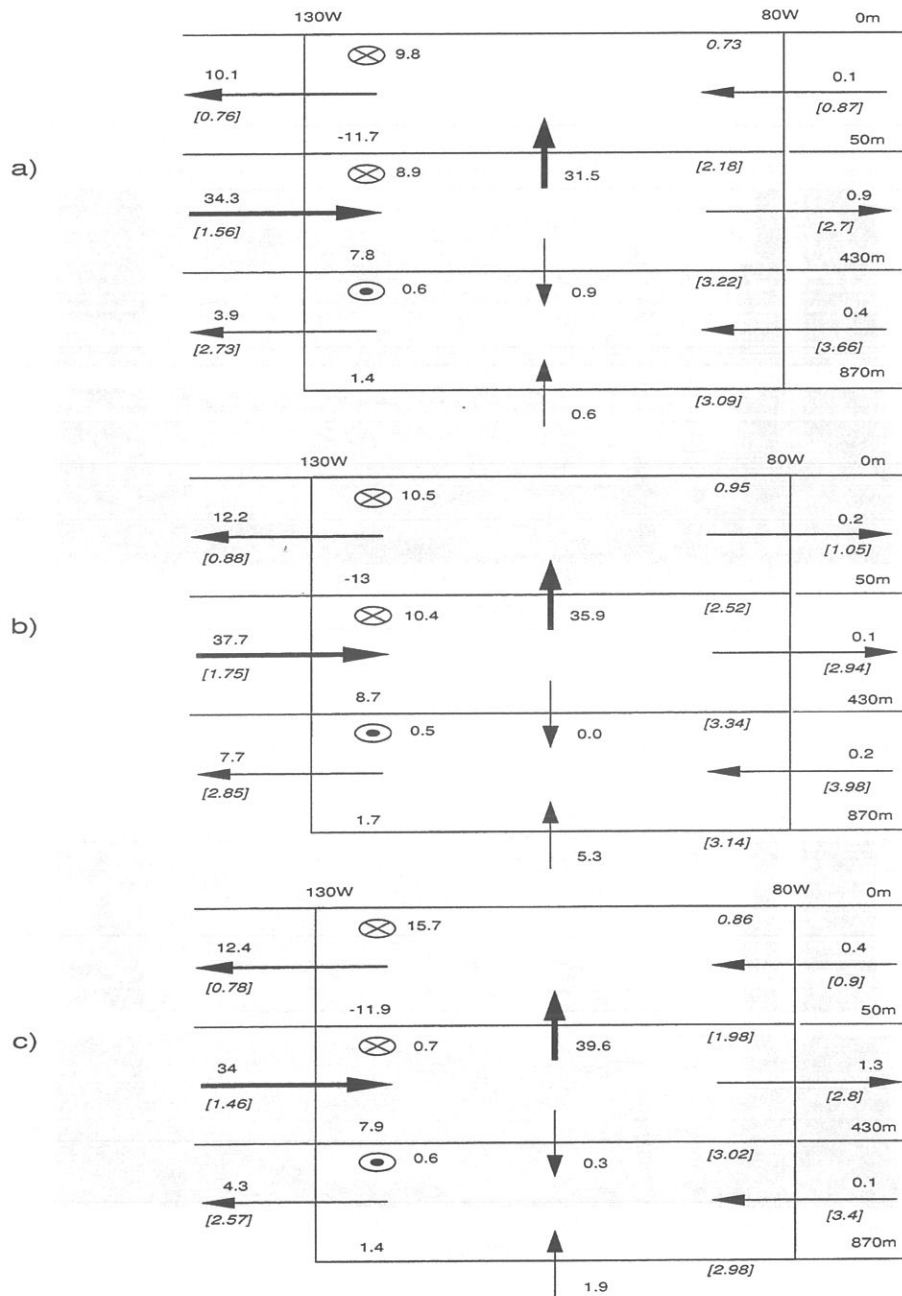


Figure 7. Annual mean total phosphorus budget for the upper 870 m in the eastern equatorial Pacific ocean. Three budgets are displayed: (a) standard case, (b) case HV, and (c) case CVD. Fluxes units are  $\text{kmol P s}^{-1}$ . Circled crosses (dots) represent meridional outfluxes (influxes). The number in the lower left corner of each box represents the flux related to biological activity. Italicized numbers in square brackets are total phosphorus concentrations averaged over each box ( $\mu\text{mol L}^{-1}$ ).

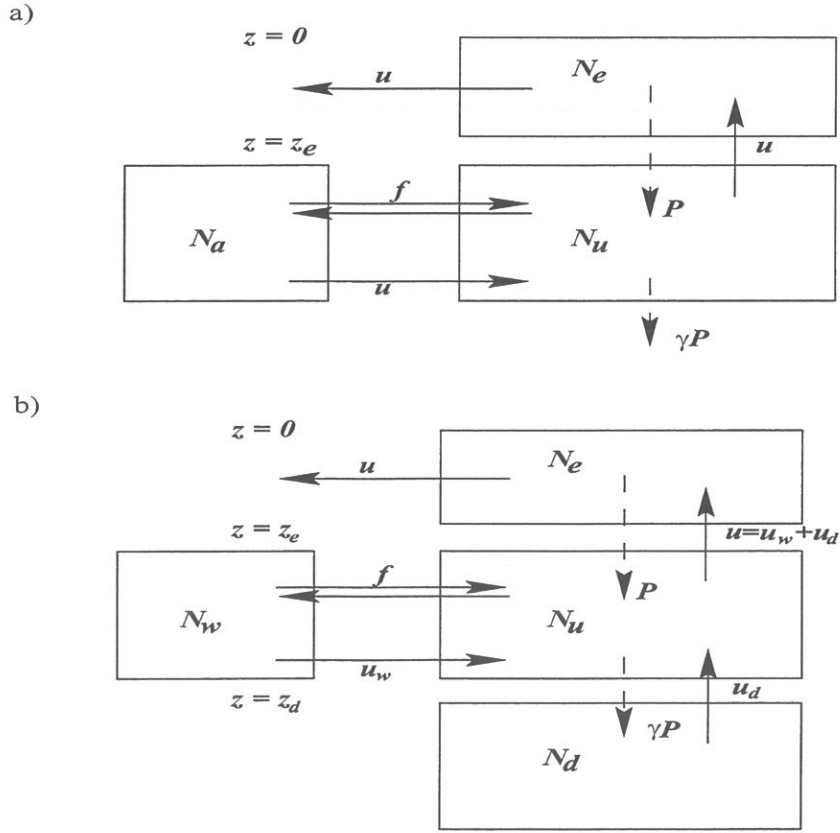


Figure 8. (a) Box model used by Najjar et al. [1992] to determine processes involved in nutrient trapping.  $N_u$ ,  $N_e$ , and  $N_a$  represent the nutrient concentrations ( $\mu\text{mol m}^{-3}$ ) of the upwelled waters, the euphotic zone, and the region from which the upwelled waters originate (ambient waters), respectively.  $P$  is the production exported below the euphotic zone ( $\text{mol s}^{-1}$ ).  $\gamma$  is the fraction of  $P$  that is not remineralized within the divergence zone.  $u$  is the intensity of the divergence ( $\text{m}^3 \text{s}^{-1}$ ) and  $f$  is the mixing intensity between the upwelled waters and the ambient waters ( $\text{m}^3 \text{s}^{-1}$ ). This figure is redrawn from Najjar et al. [1992]. (b) Revised version of Najjar et al. [1992]'s box model. The reservoir corresponding to the ambient waters is splitted into two separate reservoirs which act in an opposite way on nutrient trapping: the western Pacific and the deep ocean, whose nutrient concentrations are  $N_w$  and  $N_d$ , respectively.  $u_w$  denotes the intensity of the EUC ( $\text{m}^3 \text{s}^{-1}$ ) and  $u_d$  is the intensity of the upwelling of abyssal waters (both in  $\text{m}^3 \text{s}^{-1}$ ).  $u_s$  is the intensity of the near surface upwelling ( $\text{m}^3 \text{s}^{-1}$ ). Other processes and symbols included in this box model are identical to those in panel (a) of this figure.



## Déjà paru :

- 1 : **Janvier 1998** Agnès Ducharne, Katia Laval and Jan Polcher,  
*Sensitivity of the hydrological cycle to the parameterization of soil hydrology in a GCM*
- 2 : **Janvier 1998** Marina Lévy, Laurent Mémery and Jean-Michel André ,  
*Simulation of primary production and export fluxes in the Northwestern Mediterranean Sea*
- 3 : **Février 1998** Valérie Masson, Sylvie Joussaume, Sophie Pinot and Gilles Ramstein, *Impact of parameterizations on simulated winter mid-Holocene and Last Glacial Maximum climatic changes in the Northern Hemisphere*
- 4 : **Mars 1998** Jérôme Vialard et Pascale Delecluse, *An OGCM Study for the TOGA Decade. Part I: Role of Salinity in the Physics of the Western Pacific Fresh Pool, Part II: Barrier layer formation and variability*



